

Comparison of 2D topological codes and their decoding performances

Kao-Yueh Kuo and Ching-Yi Lai

Institute of Communications Engineering, National Yang Ming Chiao Tung University, Hsinchu 300093, Taiwan.

{kykuo, cylai}@nycu.edu.tw

Abstract—Topological quantum codes are favored because they allow qubit layouts that are suitable for practical implementation. An N -qubit topological code can be decoded by minimum-weight perfect matching (MWPM) with complexity $O(\text{poly}(N))$ if it is of CSS-type. Recently it is shown that various quantum codes, including non-CSS codes, can be decoded by an adapted belief propagation with memory effects (denoted MBP) with complexity almost linear in N . In this paper, we show that various two-dimensional topological codes, CSS or non-CSS, regardless of the layout, can be decoded by MBP, including color codes and twisted XZZX codes. We will comprehensively compare these codes in terms of code efficiency and decoding performance, assuming perfect error syndromes.

I. INTRODUCTION

Quantum codes can be understood as codes over $\text{GF}(4)$ [1]. We consider error operators that are tensor products of Pauli matrices $I = \begin{bmatrix} 1 & 0 \\ 0 & 1 \end{bmatrix}$, $X = \begin{bmatrix} 0 & 1 \\ 1 & 0 \end{bmatrix}$, $Z = \begin{bmatrix} 1 & 0 \\ 0 & -1 \end{bmatrix}$, and $Y = iXZ$. Let $X_j = I^{\otimes(j-1)} \otimes X \otimes I^{\otimes(N-j)}$ and similarly for Z_j . Then $\{X_j, Z_j\}_{j=1}^N$ together with $iI^{\otimes N}$ generate the N -fold Pauli group \mathcal{G}_N . An abelian subgroup of \mathcal{G}_N that does not contain $-I^{\otimes N}$ is called a stabilizer group and its elements are stabilizers. A stabilizer group with $N - K$ independent generators defines an $[[N, K, D]]$ quantum stabilizer code, which encodes K information qubits into N physical qubits, and D is the minimum distance of the code. The code space is the joint $+1$ eigenspace of the stabilizers, and we can regard the stabilizer group as “parity checks” for this quantum code. For basics of stabilizer codes, please refer to [1]–[3].

A Calderbank–Shor–Steane (CSS) code is a stabilizer code with a set of independent stabilizer generators that are all Pauli X s or Z s [4], [5]. They are of interest for fault-tolerant quantum computation (FTQC). Moreover, CSS codes can be treated as classical binary codes and X and Z errors are separately decoded in a suboptimal way.

A topological code is a stabilizer code, where the composed qubits are placed on a lattice and only local interactions between qubits are required. A stabilizer generator is defined by a plaquette (or called face) and it operates nontrivially on only the vertices (qubits) of the plaquette. Thus stabilizer measurements can be locally done, which is a desirable feature for some technologies, such as superconducting qubits. Note that only a subset of the stabilizers defined by all the plaquettes are independent. Since stabilizers will be constantly measured in error correction, the time cost for stabilizer measurements

affects the decoding complexity. Thus low-weight stabilizer generators are favored. We will consider the average and maximum weight of stabilizer generators that will be measured, denoted by w_{avg} and w_{max} , respectively.

If a family of $[[N, K, D]]$ codes has a two-dimensional (2D) lattice representation, the code parameters must satisfy the Bravyi–Poulin–Terhal (BPT) bound [6]

$$N \geq KD^2/c \quad (1)$$

for a certain c . This number c characterizes the “efficiency” of the code family and a code family with large c is desirable.

In general, a topological code is degenerate and has many low-weight stabilizers. The minimum distance does not necessarily characterize its error performance and one has to see the its performance over a noisy channel using a decoding procedure. A related notion is the error *threshold* of the combination of a code family and a decoding procedure, which is defined as the physical error rate, below which the logical error rate can be arbitrarily decreased by increasing the lattice size [7]–[10]. Usually a higher threshold is desirable.

Kitaev proposed a family of toric codes with qubits placed on the surface of a torus [11]. A toric code has two types of stabilizer generators $XXXX$ or $ZZZZ$ operating on the four vertices of a plaquette (c.f. Fig. 1(a)). Toric codes satisfy the BPT bound with $c = 1$. For higher code rate (higher c), one may also consider rotated toric codes [12], [13] (c.f. Fig. 2).

Since the torus layout may not be physically implemented, a 2D planar lattice is desirable and surface codes (c.f. Fig. 1(b)) and color codes (c.f. Fig. 4) are thus introduced [14], [15]. Surface codes have a rectangular layout. Color codes, with non-rectangular layouts, have higher efficiency than surface codes but they have stabilizer generators of higher weight.

For a higher ratio of D^2/N , one may consider non-CSS topological codes. A specific type of codes is defined by a weight-four stabilizer generator $XZZX$ operating on each plaquette of a lattice [16], [17]. The smallest $XZZX$ code is the well-known $[[5, 1, 3]]$ code [2], [18] when described on a twisted torus (see Fig. 6(a)). However, the decoding of an $XZZX$ code may be more complicated since it is non-CSS.

We will compare the toric, surface, color, and $XZZX$ codes in this paper in the perspectives of efficiency, stabilizer weight, decoding performance and complexity. We consider decoding by the minimum-weight perfect matching (MWPM) [19] and the refined belief propagation with memory effects (MBP) [20]. (See [21] for some basics of BP decoding of quantum

KYK and CYL were supported by the Ministry of Science and Technology (MOST) in Taiwan, under Grant MOST110-2628-E-A49-007.

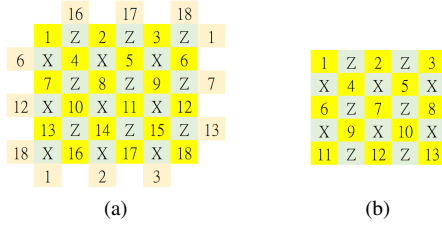


Fig. 1. (a) The lattice of a $[[2L^2, 2, L]]$ toric code for $L = 3$. (b) The lattice of a $[[2L^2 - 2L + 1, 1, L]]$ surface code for $L = 3$. Each data qubit is represented by a yellow box labeled by a number, from 1 to N . Each green box with label $W \in \{X, Z\}$ surrounded by four data qubits i, j, k, l represents a stabilizer $W_i W_j W_k W_l$. In (a), each orange box on the boundary represents the yellow box with the same label and it is used to indicate the connection of qubits since the lattice is on the surface of a torus. For example, the label Z surrounded by qubits 1, 2, 4, 16 represents $Z_1 Z_2 Z_4 Z_{16}$. In (b), some qubits and stabilizers in (a) are deleted to create physical boundaries. Thus there are no wrapped connections and the boundary stabilizers are of weight three, e.g., the label X surrounded by qubits 1, 4, 6 represents $X_1 X_4 X_6$.

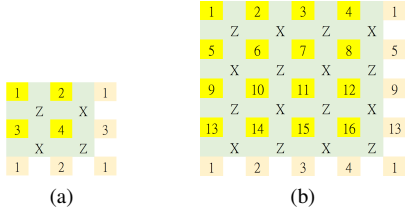


Fig. 2. The lattices of $[[L^2, 2, L]]$ rotated toric codes for even $L \geq 2$: (a) $L = 2$ and (b) $L = 4$. The labels are similarly defined as in Fig. 1.

codes.) In particular, MBP achieves a threshold of 17.5% for many code families, compared to 15.5% by MWPM. The results are summarized in Tables I and II.

We review CSS and non-CSS topological codes in Secs. II and III, respectively, and compare the codes in Table I. Their decoding performances are discussed in Sec. IV, and a summary is given in Table II. Then we conclude in Sec. V.

II. CSS TOPOLOGICAL CODES

A. Toric codes

The family of Kitaev's $[[2L^2, 2, L]]$ toric codes has a lattice representation on the surface of a torus [11], as shown in Fig. 1(a) for $L = 3$. Note that the toric codes have wrapped boundaries (or say, no physical boundaries). The toric codes saturate the BPT bound with efficiency $c = 1$.

A family of $[[L^2, 2, L]]$ rotated toric codes with $c = 2$ for even $L \geq 2$ has a similar lattice representation [12], [13], as shown in Fig. 2 for $L = 2$ and 4. Note that labels Z and X are alternated on each row or column of the lattice.

Both toric and rotated toric codes have $w_{\max} = w_{\text{avg}} = 4$.

B. Surface codes

The lattice of a toric code is defined on the 2D surface of a torus. One can similarly define a lattice on the 2D surface of a plane, by deleting some qubits and stabilizers in a toric code to create physical (or called *open*) boundaries [14]. This results in a family of $[[2L^2 - 2L + 1, 1, L]]$ surface codes, as shown in Fig. 1(b) for $L = 3$. Since surface codes have a planar lattice,

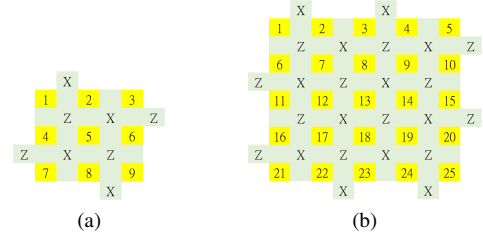


Fig. 3. The lattice of $[[L^2, 1, L]]$ rotated surface codes for odd $L \geq 3$: (a) $L = 3$ and (b) $L = 5$. The labels are similarly defined as in Fig. 1.

they are more suitable for physical implementation. However, the surface codes have lower efficiency $c \approx 1/2$.

Similarly, a family of $[[L^2, 1, L]]$ rotated surface codes for odd $L \geq 3$ has higher efficiency $c = 1$ [12], [13], as shown in Fig. 3 for $L = 3$.

Both unrotated and rotated surface codes have $w_{\max} = 4$ and $w_{\text{avg}} \approx 4$ (asymptotically).

C. Color Codes

Color codes also have a planar structure like the surface codes [15] and three families of color codes are discussed here, as in Fig. 4 and [22, Fig. 2(c)]. They are designed to have better efficiency c at the cost of larger stabilizer weights.

A color code is represented by a graph composed of three types of plaquettes (indicated by three colors: red, green, and blue). A data qubit is placed on each vertex in the graph. A plaquette defines both an X -type stabilizer and a Z -type stabilizer, with an X or Z on each of its vertices. There are two rules to build colorful plaquettes. First, a plaquette and any of its adjacent plaquettes share two vertices; second, two adjacent plaquettes have different colors. The two rules guarantee that the generated stabilizers commute with each other.

The color codes in Fig. 4 and [22, Fig. 2(c)] are $[[N, 1, D]]$ codes with odd D :

- The (6,6,6) structure has $N = (3D^2 + 1)/4$ and stabilizer weights $w_{\max} = 6$ and $w_{\text{avg}} \approx 6$.
- The (4,8,8) structure has smaller $N = (D^2 + 2D - 1)/2$ but larger $w_{\max} = 8$ and $w_{\text{avg}} = (4 + 8 + 8)/3 \approx 6.67$.
- The (4,6,12) structure has $N = (3D^2 - 6D + 5)/2$ and larger $w_{\max} = 12$ and $w_{\text{avg}} = (4 + 6 + 12)/3 \approx 7.33$.

III. NON-CSS TORIC CODES

To have topological codes with higher ratio of D^2/N , non-CSS topological codes are studied. A plaquette defines X -type or Z -type stabilizers for CSS topological codes. Non-CSS stabilizers can be similarly defined by plaquettes [16], [17] but care needs to be taken for commutation relations. Some general constructions are provided in [23]. Herein, we consider the XZZX codes in [16], where each code has a rectangular layout rotated by a special angle. We provide an interpretation of a twisted torus by combining two regular squared lattices to illustrate the structure of a twisted XZZX code.

Recall that a rotated structure has better efficiency. One can use a lattice like that in Fig. 2 to define a non-CSS code but

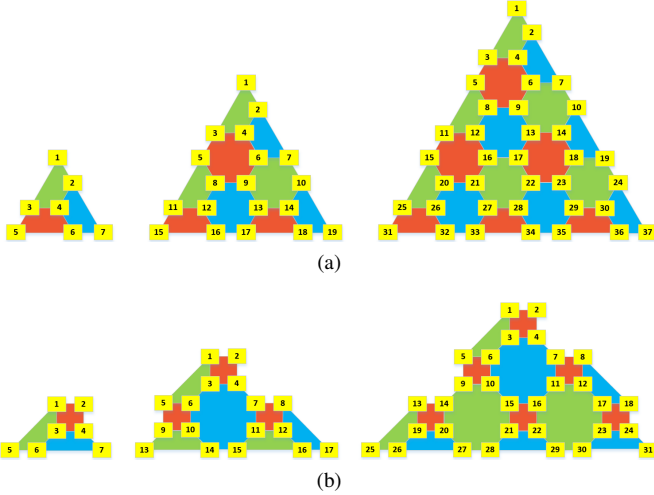


Fig. 4. The structures of (a) (6,6,6) color codes and (b) (4,8,8) color codes, for $D = 3, 5, 7$ in each subfigure. There is another typical structure of (4,6,12) color codes, as shown in [22, Fig. 2(c)]. Each color plaquette defines both an X -type stabilizer and a Z -type stabilizer. For example, the green plaquette in subfigure (a) defines two stabilizers $X_1X_2X_3X_4$ and $Z_1Z_2Z_3Z_4$.

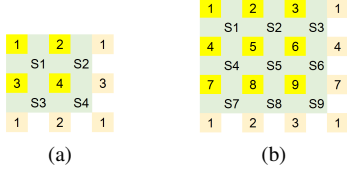


Fig. 5. The lattice of $[[L^2, 2 - (L\%2), L]]$ XZZX toric codes for (a) $L = 2$ and (b) $L = 3$. The labels are similarly defined as in Fig. 1. Label $S\#$ represents a stabilizer $X_iZ_jZ_kX_l$ in the four vertices i, j, k, l on the left-upper, right-upper, left-lower, right-lower corners, respectively. For example, $S1$ in (a) is $X_1Z_2Z_3X_4$, and $S9$ in (b) is $X_9Z_7Z_3X_1 = X_1Z_3Z_7X_9$.

each plaquette defines a stabilizer of the form $X_iZ_jZ_kX_l$. This leads to the family of $[[L^2, 2 - (L\%2), L]]$ XZZX toric codes for $L \geq 2$ as shown in Fig. 5. This family of codes satisfy the BPT bound with $c = 2$ for even L and $c = 1$ for odd L . Note the XZZX toric codes can be defined for $L \geq 2$ but rotated toric codes are only defined for even L .

XZZX surface codes can be similarly defined by a lattice structure as in Fig. 3.

To have XZZX codes with higher D^2/N , one can adjust the connections of the wrapped boundaries of an $L \times L$ torus lattice as follows. Let J denote an integer twist offset so that the wrapped boundaries have a shift J [24]–[29]. J has to be coprime with L , i.e., $\gcd(L, J) = 1$, such that J generates all the elements in $\mathbb{Z}_L = \{0, 1, 2, \dots, L - 1\}$. For example, a twist offset $J = 1$ in the wrapped boundaries is shown in Fig. 6. In addition, a $J \times J$ lattice needs to be attached to the $L \times L$ lattice so that we have a wrapped structure. For $J = 1$, this is illustrated in Fig. 6(a) with qubit 5 and stabilizer $S5$, or in Fig. 6(b) with qubit 10 and stabilizer $S10$. An example of twist offset $J = 2$ is shown in Fig. 7.

To sum up, we have a family of $[[N = L^2 + J^2, K, D]]$ twisted XZZX codes, where $\gcd(L, J) = 1$, $K = 2$, $D = L$ for even N , and $K = 1$, $D = L + J$ for odd N . We remark

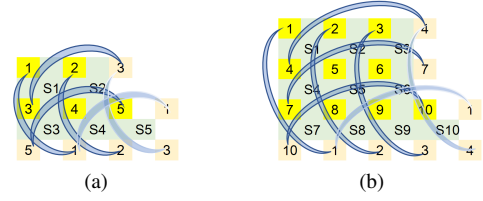


Fig. 6. The lattice of twisted XZZX codes with twist $J = 1$ for (a) $L = 2$ and (b) $L = 3$. The labels are similarly defined as in Fig. 5. The (blue) arcs indicate the connections of the wrapped boundaries.

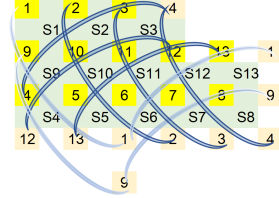


Fig. 7. The lattice of a twisted XZZX code with twist $J = 2$ for $L = 3$, which corresponds to a $[[13, 1, 5]]$ code with stabilizers cyclicly generated by $X_1Z_2Z_9X_{10}$. The labels are defined similarly as in Fig. 6.

that such a twisted XZZX code has its stabilizer generators that can be cyclicly generated. For example, the stabilizers in Figs. 6(a) and (b) can be cyclicly generated by $X_1Z_2Z_3X_4$ and $X_1Z_2Z_4X_5$, respectively. (As a quantum code is like an additive code, the corresponding classical codes over $\text{GF}(4)$ is not necessarily a cyclic linear code.)

For $J = L - 1$, we have a family of twisted XZZX codes with parameters $[[\frac{(D^2 + 1)}{2}, 1, D]]$ for $D = 2L - 1$ for any integer $L \geq 2$. This family of codes satisfy the BPT bound with efficiency $c \approx 2$. The smallest nontrivial code in this family is the unique $[[5, 1, 3]]$ code in Fig. 6(a).

Obviously, the twisted XZZX codes have $w_{\max} = w_{\text{avg}} = 4$.

All the mentioned codes are compared in Table I. Observe that a toric code family exists with good efficiency $c = 2$ and low stabilizer weights $w_{\text{avg}} = w_{\max} = 4$. On the other hand, planar codes usually have smaller c or larger w_{avg} and w_{\max} .

IV. DECODING PERFORMANCE

We assume depolarizing errors. The threshold of a code family and a decoding procedure is estimated by the intersection point of the performance curves (see [9] or Fig. 10).

MWPM is the most widely used decoder for 2D topological codes. The threshold of toric, surface, or XZZX codes using MWPM is about 15.5% [9], and the threshold of color codes using MWPM is about 13% [30], [31]. The complexity of decoding toric and surface codes by MWPM is $O(N^2)$, but it is $O(N^3)$ for the XZZX codes [32, supplemental material] and $O(N^4)$ for the color codes [31].

We proposed MBP and it achieves thresholds close to 16% and 17.5% on the surface and toric codes, respectively, with complexity $O(N \log \log N)$ [20]. The decoding procedure is simply the syndrome-based quaternary message passing on the Tanner graph corresponding to the underlying code, CSS or non-CSS, regardless of the layout. Since MBP can handle

TABLE I
COMPARISON OF VARIOUS CODES WITH 2D TOPOLOGICAL STRUCTURES.

codes	structure	$[[N, K, D]]$	codes with $D \approx 3$	c	w_{avg}	w_{max}	planar
toric codes [11]	Fig. 1(a)	$[[2L^2, 2, L]]$	$[[18, 2, 3]]$	1	4	4	
surface codes [11], [14]	Fig. 1(b)	$[[2L^2 - 2L + 1, 1, L]]$	$[[13, 1, 3]]$	$\approx 1/2$	≈ 4	4	✓
rotated toric codes [12]	Fig. 2 (even L)	$[[L^2, 2, L]]$	$[[16, 2, 4]]$	2	4	4	
rotated surface codes [12]	Fig. 3 (odd L)	$[[L^2, 1, L]]$	$[[9, 1, 3]]$	1	≈ 4	4	✓
(6,6,6) color codes [15]	Fig. 4(a) (odd D)	$[[\frac{3}{4}D^2 + \frac{1}{4}, 1, D]]$	$[[7, 1, 3]]$	$\approx 4/3$	≈ 6	6	✓
(4,8,8) color codes [15]	Fig. 4(b) (odd D)	$[[\frac{1}{2}D^2 + D - \frac{1}{2}, 1, D]]$	$[[7, 1, 3]]$	≈ 2	≈ 6.67	8	✓
(4,6,12) color codes [15]	[22, Fig. 2(c)] (odd D)	$[[\frac{3}{2}D^2 - 3D + \frac{5}{2}, 1, D]]$	$[[7, 1, 3]]$	$\approx 2/3$	≈ 7.33	12	✓
XZZX toric codes [17]	Fig. 5	$[[L^2, 2 - (L\%2), L]]$	$[[9, 1, 3]], [[16, 2, 4]]$	$2 - L\%2$	4	4	
XZZX surface codes [17]	Fig. 3 (but plaquette XZZX)	$[[L^2, 1, L]]$	$[[9, 1, 3]]$	1	≈ 4	4	✓
XZZX twisted codes [16]	Figs. 6(a) and 7 ($J = L - 1$)	$[[D^2 + 1)/2, 1, D]]$	$[[5, 1, 3]]$	≈ 2	4	4	

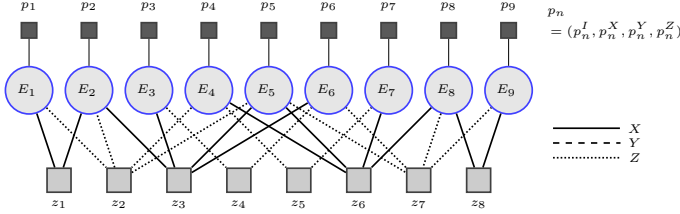


Fig. 8. The Tanner graph of the $[[9, 1, 3]]$ surface code in Fig. 3(a). $E_n \in \{I, X, Y, Z\}$ is a variable node corresponding to the Pauli error on the n -th qubit. p_n is the initial belief of E_n . $z_m \in \{0, 1\}$ is the syndrome bit of the m -th stabilizer measurement.

binary or quaternary messages, we will use MBP_4 with a subscript to emphasize that quaternary decoding is considered here [20, Algorithm 1].

MBP_4 is a message passing algorithm on the Tanner graph defined by the check matrix of a code. A check matrix S of a code is an $M \times N$ matrix over $\{I, X, Y, Z\}$, where M is the number of measured stabilizers. For example, the $[[9, 1, 3]]$ surface code in Fig. 3(a) has

$$S = \begin{bmatrix} X & X & I & I & I & I & I & I & I \\ Z & Z & I & Z & Z & I & I & I & I \\ I & X & X & I & X & X & I & I & I \\ I & I & Z & I & I & Z & I & I & I \\ I & I & I & Z & I & I & Z & I & I \\ I & I & I & X & X & I & X & X & I \\ I & I & I & I & Z & Z & I & Z & Z \\ I & I & I & I & I & I & I & X & X \end{bmatrix}$$

and the corresponding Tanner graph is shown in Fig. 8, drawn as a factor graph to also show the initial distribution p_n .

MBP_4 uses a message normalization parameter α . One can optimize the decoding performance over $\alpha \in \{1, 0.99, \dots, 0.5\}$ to select an optimum α^* , and this is referred to as adaptive MBP_4 (AMBP_4) [20, Algorithm 2].

First we consider the twisted XZZX codes with parameters $[[D^2 + 1)/2, 1, D]]$. In Fig. 9, we show that MBP_4 improves the conventional BP_4 with $\alpha = 0.7$. (We collect 100 logical errors for each data point for a figure at this scale.) The performance of AMBP_4 for $D = 23$ is also shown in Fig. 9.

We apply AMBP_4 for different D and show in Fig. 10 that the threshold of AMBP_4 on the twisted XZZX codes is close to 17.5%. (We collect 10000 logical errors for each data point for a figure at this scale.) To prevent any performance fluctuation, we use the technique of initializing p_n by a fixed depolarizing

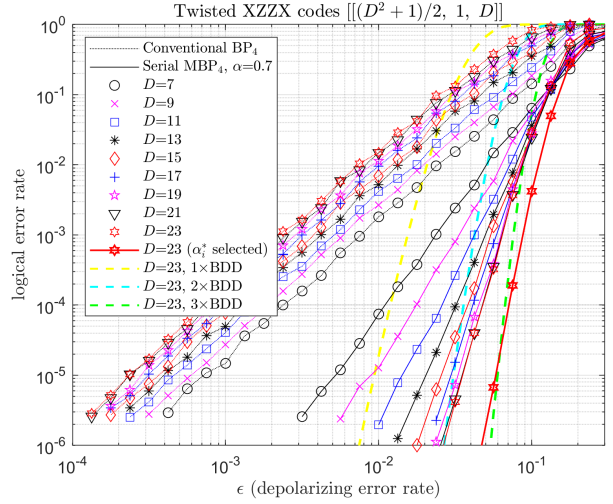


Fig. 9. MBP_4 decoding performance. Dotted lines are conventional BP_4 . Solid lines are MBP_4 with $\alpha = 0.7$, which has performance saturation effect because a fixed α is used. The bold line is AMBP_4 (which uses MBP_4 but chooses an optimum α^* and has higher complexity). Several bounded-distance-decoding (BDD) performance curves are also shown for reference.

rate ϵ_0 , i.e., fixing $p_n = (1 - \epsilon_0, \frac{\epsilon_0}{3}, \frac{\epsilon_0}{3}, \frac{\epsilon_0}{3})$ regardless of the actual ϵ . (See [20] for more discussions of this technique).

Denote the error distribution by $p = (p^I, p^X, p^Y, p^Z)$. XZZX codes are more effective for biased Pauli errors [33], but they need a tailored MWPM with complexity $O(N^3)$ due to the non-CSS plaquette [32, supplemental material]. For MBP , any distribution p can be supported and the decoding complexity remains the same. Herein, we focus on depolarizing errors for comparison. The performance curves of AMBP_4 on the XZZX toric codes defined in Fig. 5 is shown in Fig. 11. Both even L and odd L roughly achieve a threshold of 17.5%.

For color codes, MWPM needs additional processes since a stabilizer plaquette may have weight higher than four. MWPM achieves a threshold of 13.3% on the (4,8,8) color codes without specifying the complexity [30] and a threshold of 13.05% on the (6,6,6) color codes with complexity $O(N^4)$ [31]. (Decoding the (4,8,8) color codes is considered relatively harder from the trellis complexity of the code [34].) AMBP_4 , on the other hand, can decode a color code by just giving its check matrix, without additional processes. For comparison

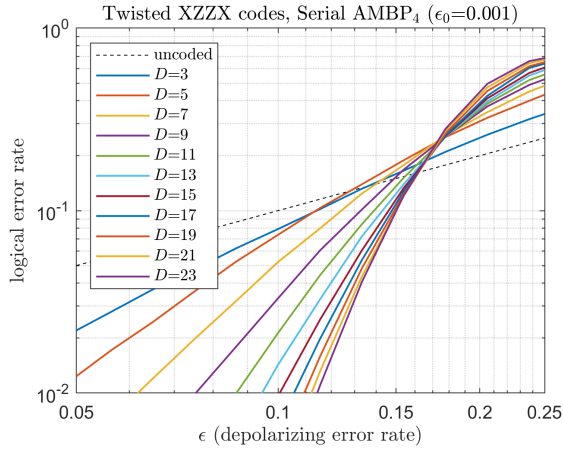


Fig. 10. The performance curves of the $[[\frac{(D^2+1)}{2}, 1, D]]$ twisted XZZX codes over depolarizing errors by AMBP₄. The intersection point of the performance curves roughly suggests a threshold of 17.5%.

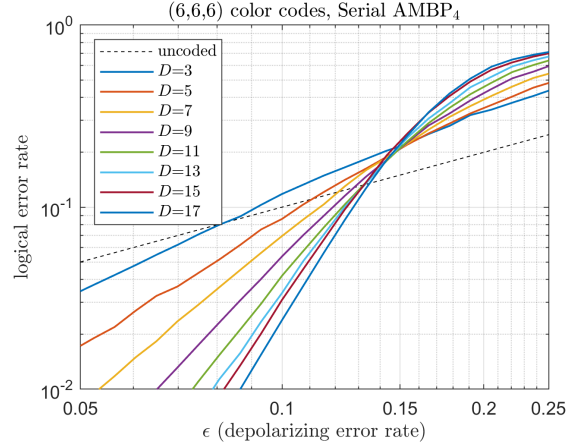


Fig. 12. The performance curves of the (6,6,6) color codes over depolarizing errors by AMBP₄, which roughly suggest a threshold of 14.5%. (For $D = 17$, p_n is initialized by a fixed $\epsilon_0 = 0.042$ to prevent the curve fluctuation.)

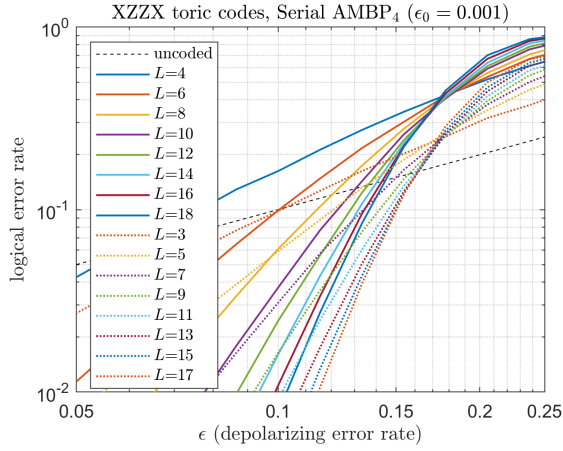


Fig. 11. The decoding performance curves of the $[[L^2, 2 - (L\%2), L]]$ XZZX toric codes over depolarizing errors by AMBP₄. Both even L (with efficiency $c = 2$) and odd L (with $c = 1$) roughly achieve a threshold of 17.5%.

in terms of complexity, we decode the (6,6,6) color codes by AMBP₄ and the performance curves roughly suggest a threshold of 14.5%, as shown in Fig. 12.

We summarize all the results in Table II.

We remark that AMBP₄ on color codes is found to have some error floor in performance, as shown in Fig. 13. Since BP is an approximation decoder, it may encounter this issue for some codes. In the fault-tolerant case using MWPM on color codes, it seems to have an error floor as well [30, Fig. 14].

V. CONCLUSION AND DISCUSSIONS

We compared various 2D topological codes (Table I) and their decoding performances by MWPM and MBP (Table II). We conclude that MBP is easier to adapt to different layouts and tends to have better performance and lower complexity.

It seems that the physical error rate of the intersection point tends to reduce if we keep increasing D . A technique that may prevent this reduction is renormalization group (RG) [35] but

TABLE II
THRESHOLDS AND COMPLEXITIES OF VARIOUS QUANTUM CODES WITH MWPM- OR BP-BASED DECODERS OVER DEPOLARIZING ERRORS.

code family	MWPM [19] threshold	complexity	AMBP ₄ [20] threshold
surface	15.5% [9]	$O(N^2)$ [10]	16%
toric	15.5% [9]	$O(N^2)$ [10]	17.5%
color	13.05% [†]	$O(N^4)$ [31]	14.5% (Fig. 12)
XZZX toric	15.5% [33]	$O(N^3)$ [32]	17.5% (Fig. 11)
XZZX twisted			17.5% (Fig. 10)

[†]: The 13.05% is rescaled from the 8.7% for the independent X - Z channel by a factor of $3/2$ [31].

The complexity of AMBP₄ is $O(N \log \log N)$ in each case, by a similar analysis as in [20].

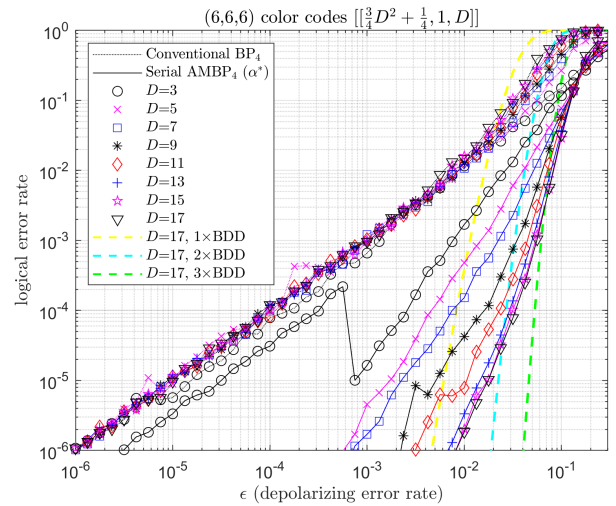


Fig. 13. The performance curves of the (6,6,6) color codes over depolarizing errors by AMBP₄. (The curve fluctuation can be prevented by using a fixed ϵ_0 to initialize p_n , but this does not improve the error-floor performance.)

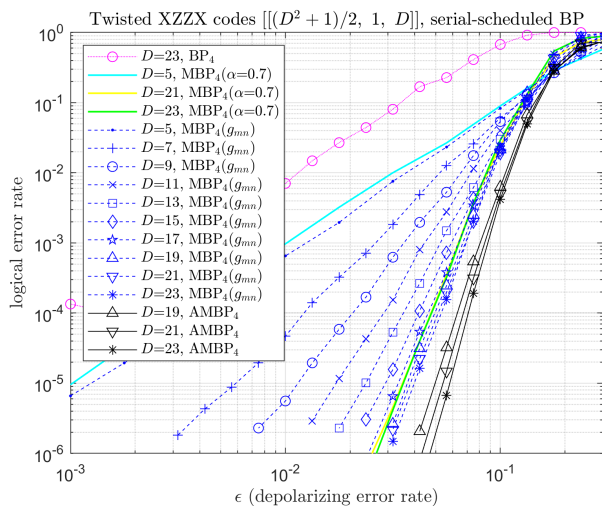


Fig. 14. MBP decoding performance. The MBP performance saturation effect (Fig. 9) can be improved by using different weight g_{mn} per edge (m, n) of the Tanner graph of the code, where the computation of g_{mn} is referred to [20, Eq. (10)]. AMBP₄ still has better performance (but higher complexity since the optimum α^* is determined by many instances of the decoder).

it needs to concern the lattice layouts. Another technique that may improve the threshold value is discussed in Appendix.

MWPM has been extended to handle measurement and gate errors in FTQC [7]–[10]. BP can be extended to correct data and measurement errors simultaneously [36]. It is interesting to consider gate errors in BP as well.

APPENDIX

Since BP can be seen as a recurrent neural network (RNN), for MBP₄, if the weight of each edge (g_{mn}) can be determined per iteration [20, Eq. (10)], then the decoder will perform better than MBP₄ with a fixed α , as shown in Fig. 14. Note that AMBP₄ still has better performance, which means that the thresholds of AMBP₄ shown in this paper can be further improved by determining optimum g_{mn}^* per edge per iteration (which may be possibly done by pre-training).

REFERENCES

- [1] A. R. Calderbank, E. M. Rains, P. W. Shor, and N. J. A. Sloane, “Quantum error correction via codes over GF(4),” *IEEE Trans. Inf. Theory*, vol. 44, pp. 1369–1387, 1998.
- [2] D. Gottesman, “Stabilizer codes and quantum error correction,” Ph.D. dissertation, California Institute of Technology, 1997.
- [3] M. A. Nielsen and I. L. Chuang, *Quantum Computation and Quantum Information*. Cambridge University Press, 2000.
- [4] A. R. Calderbank and P. W. Shor, “Good quantum error-correcting codes exist,” *Phys. Rev. A*, vol. 54, p. 1098, 1996.
- [5] A. M. Steane, “Error correcting codes in quantum theory,” *Phys. Rev. Lett.*, vol. 77, p. 793, 1996.
- [6] S. Bravyi, D. Poulin, and B. Terhal, “Tradeoffs for reliable quantum information storage in 2D systems,” *Phys. Rev. Lett.*, vol. 104, p. 050503, 2010.
- [7] E. Dennis, A. Kitaev, A. Landahl, and J. Preskill, “Topological quantum memory,” *J. Math. Phys.*, vol. 43, pp. 4452–4505, 2002.
- [8] R. Raussendorf, J. Harrington, and K. Goyal, “A fault-tolerant one-way quantum computer,” *Ann. Phys.*, vol. 321, pp. 2242–2270, 2006.
- [9] D. S. Wang, A. G. Fowler, A. M. Stephens, and L. C. L. Hollenberg, “Threshold error rates for the toric and planar codes,” *Quant. Inf. Comput.*, vol. 10, pp. 456–469, 2010.

- [10] A. G. Fowler, A. C. Whiteside, and L. C. Hollenberg, “Towards practical classical processing for the surface code,” *Phys. Rev. Lett.*, vol. 108, p. 180501, 2012.
- [11] A. Y. Kitaev, “Fault-tolerant quantum computation by anyons,” *Ann. Phys.*, vol. 303, pp. 2–30, 2003.
- [12] H. Bombín and M. A. Martin-Delgado, “Optimal resources for topological two-dimensional stabilizer codes: Comparative study,” *Phys. Rev. A*, vol. 76, p. 012305, 2007.
- [13] C. Horsman, A. G. Fowler, S. Devitt, and R. Van Meter, “Surface code quantum computing by lattice surgery,” *New J. Phys.*, vol. 14, p. 123011, 2012.
- [14] S. B. Bravyi and A. Y. Kitaev, “Quantum codes on a lattice with boundary,” *e-print quant-ph/9811052*, 1998.
- [15] H. Bombin and M. A. Martin-Delgado, “Topological quantum distillation,” *Phys. Rev. Lett.*, vol. 97, p. 180501, 2006.
- [16] A. A. Kovalev, I. Dumer, and L. P. Pryadko, “Design of additive quantum codes via the code-word-stabilized framework,” *Phys. Rev. A*, vol. 84, p. 062319, 2011.
- [17] B. Terhal, F. Hassler, and D. DiVincenzo, “From Majorana fermions to topological order,” *Phys. Rev. Lett.*, vol. 108, p. 260504, 2012.
- [18] R. Lafamme, C. Miquel, J. P. Paz, and W. H. Zurek, “Perfect quantum error correcting code,” *Phys. Rev. Lett.*, vol. 77, pp. 198–201, 1996.
- [19] J. Edmonds, “Paths, trees, and flowers,” *Canadian Journal of Mathematics*, vol. 17, pp. 449–467, 1965.
- [20] K.-Y. Kuo and C.-Y. Lai, “Exploiting degeneracy in belief propagation decoding of quantum codes,” *e-print arXiv:2104.13659*, 2021.
- [21] —, “Refined belief propagation decoding of sparse-graph quantum codes,” *IEEE J. Sel. Areas Inf. Theory*, vol. 1, pp. 487–498, July 2020.
- [22] A. J. Landahl, J. T. Anderson, and P. R. Rice, “Fault-tolerant quantum computing with color codes,” *e-print arXiv:1108.5738*, 2011.
- [23] R. Sarkar and T. J. Yoder, “A graph-based formalism for surface codes and twists,” *e-print arXiv:2101.09349*, 2021.
- [24] H. Bombín, “Topological order with a twist: Ising anyons from an Abelian model,” *Phys. Rev. Lett.*, vol. 105, p. 030403, 2010.
- [25] B. J. Brown, S. D. Bartlett, A. C. Doherty, and S. D. Barrett, “Topological entanglement entropy with a twist,” *Phys. Rev. Lett.*, vol. 111, p. 220402, 2013.
- [26] M. B. Hastings and A. Geller, “Reduced space-time and time costs using dislocation codes and arbitrary ancillas,” *e-print arXiv:1408.3379*, 2014.
- [27] T. J. Yoder and I. H. Kim, “The surface code with a twist,” *Quantum*, vol. 1, p. 2, 2017.
- [28] D. Litinski and F. von Oppen, “Quantum computing with Majorana fermion codes,” *Phys. Rev. B*, vol. 97, p. 205404, 2018.
- [29] M. S. Kesselring, F. Pastawski, J. Eisert, and B. J. Brown, “The boundaries and twist defects of the color code and their applications to topological quantum computation,” *Quantum*, vol. 2, p. 101, 2018.
- [30] D. S. Wang, A. G. Fowler, C. D. Hill, and L. C. L. Hollenberg, “Graphical algorithms and threshold error rates for the 2d color code,” *Quantum Inf. Comput.*, vol. 10, pp. 780–802, 2010.
- [31] N. Delfosse, “Decoding color codes by projection onto surface codes,” *Phys. Rev. A*, vol. 89, p. 012317, 2014.
- [32] D. K. Tuckett, S. D. Bartlett, S. T. Flammia, and B. J. Brown, “Fault-tolerant thresholds for the surface code in excess of 5% under biased noise,” *Phys. Rev. Lett.*, vol. 124, p. 130501, 2020.
- [33] J. Bonilla Ataides, D. Tuckett, S. Bartlett, S. Flammia, and B. Brown, “The XZZX surface code,” *Nat. Commun.*, vol. 12, pp. 1–12, 2021.
- [34] E. Sabo, A. B. Alohious, and K. R. Brown, “Trellis decoding for qudit stabilizer codes and its application to qubit topological codes,” *arXiv preprint arXiv:2106.08251*, 2021.
- [35] G. Duclos-Cianci and D. Poulin, “Fast decoders for topological quantum codes,” *Phys. Rev. Lett.*, vol. 104, p. 050504, 2010.
- [36] K.-Y. Kuo, I.-C. Chern, and C.-Y. Lai, “Decoding of quantum data-syndrome codes via belief propagation,” in *Proc. IEEE Int. Symp. Inf. Theory (ISIT)*, 2021, pp. 1552–1557.